Available online at www.sciencedirect.com
ScienceDirect
Journal of Computational Physics 226 (2007) 1408–1431
JOURNAL OF COMPUTATIONAL PHYSICS
www.elsevier.com/locate/jcp

A lattice-Boltzmann relaxation scheme for coupled convection–radiation systems

Mapundi K. Banda [a,*], Axel Klar [b], Mohammed Seaïd [b]

[a] School of Mathematical Sciences, University of KwaZulu-Natal, Private Bag X01, Scottsville, 3209 Pietermaritzburg, South Africa
[b] AG Technomathematik, Fachbereich Mathematik, Technische Universität Kaiserslautern, 67663 Kaiserslautern, Germany

Received 16 November 2006; received in revised form 17 April 2007; accepted 25 May 2007
Available online 12 June 2007

Abstract

The convection–radiation effects in thermal fluid flows are studied based on the lattice-Boltzmann method. Nine-velocity flow and temperature distributions are used to obtain the mass, momentum and energy equations in thermal incompressible flows by studying equivalent moment systems. The radiative heat flux in the energy equation is obtained using the discrete-ordinates solution of the radiative transfer equation. A non-oscillatory relaxation scheme is used to solve the coupled moment equations. Such schemes have the advantage of being simple and easy to implement. Numerical results are presented for two test examples on coupled convection–radiation flows in two dimensional enclosures. Detailed simulation results at different flow and radiative regimes, as well as benchmark solutions, are presented and discussed.

Keywords: Lattice-Boltzmann method; Relaxation scheme; Radiative heat transfer; Natural convection; Forced convection; Incompressible Navier–Stokes equations

1. Introduction

Many kinetic equations or discrete-velocity models of kinetic equations yield, in the limit for small Knudsen and Mach numbers, an approximation of the incompressible Navier–Stokes equations. A classical example is given by the discrete-velocity models used for lattice-Boltzmann methods, see [6,9,20,13,10,8] among others. These discrete-velocity models can be viewed as relaxation systems for the incompressible Navier–Stokes equations. For such flows, pressure variations occurring are small such that variations in density can be ignored. Density variations can also be caused by changes in temperature and such variations can not, in general, be neglected. Even at small velocities, density of non-uniformly heated fluid cannot be assumed constant [28,29]. In this paper we develop a computational approach for fluid flows with temperature changes. In our investigation lattice-Boltzmann approaches are considered, see also [18,19,31,41] and references therein. A relaxation system for incompressible Navier–Stokes equations coupled with heat transport and radiation is

* Corresponding author. Tel.: +27 33 2605785; fax: +27 260 5648.
E-mail addresses: bandamk@ukzn.ac.za (M.K. Banda), klar@itwm.fhg.de (A. Klar), seaid@mathematik.uni-kl.de (M. Seaïd).

0021-9991/$ - see front matter
doi:10.1016/j.jcp.2007.05.030

developed. A similar approach for the isothermal incompressible Navier–Stokes equations and turbulent flows based on large-eddy simulation were presented in [3,4].

Relaxation type schemes have been successfully used to discretize such relaxation systems. In particular, a large number of numerical methods for kinetic equations with stiff relaxation terms have been considered in fluid dynamics or diffusive limits. For such relaxation methods and asymptotic-preserving methods, we refer to [1,7,24,26] among others. We mention here that, in the context of hyperbolic conservations laws, relaxation schemes are closely related to central schemes in the sense that both approaches provide efficient high resolution and Riemann-solver free numerical methods.

The aim of the present paper is to present a methodology for developing computational schemes for incompressible Navier–Stokes equations coupled with heat energy transport equation coupled with radiative transfer. Such a relaxation system is derived from a lattice-Boltzmann type discrete-velocity model with diffuse scaling. For energy transport a separate relaxation system is also derived. The lattice-Boltzmann method is used as a platform for developing models for thermal flows because of its physical underpinning. Such an approach gives relaxation systems that are based on physics rather than a pure mathematical formulation. This provides a consistent tool for deriving relaxation systems especially for practitioners in the applied sciences. We would like to point out that the schemes presented here consider an energy equation with all modes of energy transport namely, convection, conduction and radiation. The analytical derivations also demonstrate a relationship between the lattice-Boltzmann method and such relaxation-based schemes. Moreover, such a multiscale approach provides a natural tool for solving microscopic and macroscopic models with the same underlying model. For example, in nanoscale models for natural convection in microchips or semiconductors the microscopic model would be preferable.

We also point out that the advantage of using such a kinetic or lattice Boltzmann approach is that it provides a simple, clear and consistent framework from which relaxation systems and their high-order relaxation schemes can be developed. Such an approach for solving incompressible flow coupled to a heat equation with radiative transfer has not been documented in the literature up to now. We develop high-order relaxation methods in a straight-forward manner by discretizing relaxation systems, see Section 3. In our approach we have coupled the advection–diffusion equation with the flow equations. The main results presented in this paper are, therefore, a numerical approach based on synthesizing different schemes applied to a coupled system of radiating thermal incompressible flow models. For the first time we have designed a numerical approach that synthesizes different approaches for different models based on a common multi-scale Boltzmann-type model. This approach is simple, practical and very accurate for such problems as the test cases in Section 4 demonstrate.

To demonstrate the performance of this approach a third-order relaxation scheme is used for the flow equations. The scheme works with uniform accuracy with respect to the Knudsen and Mach numbers [3]. In the low-Mach number limit it reduces to a third-order explicit scheme for the incompressible Navier–Stokes/Boussinesq equations. This is achieved by combining the ideas developed in [27] with a third-order non-oscillatory spatial discretization and an Implicit–Explicit (IMEX) Runge–Kutta time discretization [3]. To obtain a discretization of the limit incompressible Navier–Stokes/Boussinesq equations, one can use the above-mentioned spatial discretization on the relaxation system and apply any high-order time discretization directly to the resulting semi-discrete relaxed schemes. This allows us to obtain high-order incompressible Navier–Stokes solvers with better stability properties. To solve the radiative transfer equation we formulate the discrete-ordinates method along with a diffusion-synthetic acceleration procedure. This approach can also be viewed as a discrete-velocity model for the kinetic radiative transfer.

Nowadays, many practical applications involving high temperature regimes, like convection in a glass melting furnace or the crystal growth, require the extension of the underlying flow equations such that radiation effects are included. In the problems we consider, here fluid flow is mainly defined by the limit of the incompressible Navier–Stokes equations i.e., the flow is driven by density differences at small Mach numbers. In general temperature variations are significant. Hence transport properties vary with temperature. The energy and momentum equations are now coupled and must be solved simultaneously. The second effect of temperature variation is that density variation interacts with gravity creating a body force that may modify the flow structures considerably and may be the main driving force in the flow. The latter is mainly referred to as buoyancy-driven or natural convection. The relative importance of forced convection

and buoyancy effects is measured by the ratio of the Rayleigh number Ra and the Reynolds number Re. If the Re/Ra is very large the effects of natural convection may be ignored. In purely buoyancy-driven flows it may be possible to ignore density variations in all terms except for the body force in the vertical momentum equation.

The rest of the paper is organized in the following way. Section 2 contains the lattice-Boltzmann type discrete-velocity model and its equivalent associated closed moment system relaxing to the incompressible Navier–Stokes/Boussinesq equations. Some simplified relaxation systems are also presented. In particular we introduce a simplified relaxation system that is suitable to provide relaxed schemes for the thermal incompressible Navier–Stokes equations. Section 3 describes numerical methods and solution procedures for flow system and radiative transfer equation. Finally, Section 4 presents a numerical investigation of the schemes for two test examples on natural and forced convection–radiation problems. Concluding remarks are presented in Section 5.

2. Discrete-velocity models for thermal flows and simplified relaxation systems

2.1. Lattice-Boltzmann moment system for the incompressible Navier–Stokes with a source term

The two-dimensional kinetic equation

$$\frac{\partial f}{\partial t} + \mathbf{v}\cdot\nabla f = J(f) + F, \tag{2.1}$$

describes the evolution of a particle density $f(\mathbf{x},\mathbf{v},t)$ with $\mathbf{x} = (x,y)^{\mathrm{T}} \in \mathbb{R}^2$ and $\mathbf{v} = (v_1,v_2)^{\mathrm{T}} \in \mathbb{R}^2$. The left-hand side of Eq. (2.1) represents free transport of the particles while the right-hand side describes interactions through collisions, $J(f)$, and a forcing term, F. For the two-dimensional discrete models we have

$$\mathbf{v} \in \{\mathbf{c}_0,\ldots,\mathbf{c}_{N-1}\}, \quad \mathbf{c}_i \in \mathbb{R}^2.$$

Here, we consider a model with nine velocities ($N = 9$)

$$\mathbf{c}_1 = \begin{pmatrix}1\\0\end{pmatrix}, \quad \mathbf{c}_2 = \begin{pmatrix}0\\1\end{pmatrix}, \quad \mathbf{c}_3 = \begin{pmatrix}-1\\0\end{pmatrix}, \quad \mathbf{c}_4 = \begin{pmatrix}0\\-1\end{pmatrix},$$
$$\mathbf{c}_5 = \begin{pmatrix}1\\1\end{pmatrix}, \quad \mathbf{c}_6 = \begin{pmatrix}-1\\1\end{pmatrix}, \quad \mathbf{c}_7 = \begin{pmatrix}-1\\-1\end{pmatrix}, \quad \mathbf{c}_8 = \begin{pmatrix}1\\-1\end{pmatrix},$$

and $\mathbf{c}_0 = \mathbf{0}$. In the discrete case, the $\mathbf{v}$-dependence of the particle distribution $f(\mathbf{x},\mathbf{v},t)$ is uniquely determined through N functions

$$f_i(\mathbf{x},t) = f(\mathbf{x},\mathbf{c}_i,t), \quad i = 0,\ldots,N-1.$$

Macroscopic quantities like mass-, momentum- or energy-density are obtained by taking velocity moments of f. If ζ is any $\mathbf{v}$-dependent function, we denote the discrete-velocity integral by

$$\langle\zeta\rangle = \sum_{i=0}^{N-1}\zeta(\mathbf{c}_i).$$

Mass and momentum density are then given by

$$\rho(\mathbf{x},t) = \langle f(\mathbf{x},\mathbf{v},t)\rangle \quad \text{and} \quad \rho\mathbf{u}(\mathbf{x},t) = \langle \mathbf{v} f(\mathbf{x},\mathbf{v},t)\rangle. \tag{2.2}$$

In what follows we denote the components of the velocity by $\mathbf{u} = (u_1,u_2)^{\mathrm{T}}$. In most lattice-Boltzmann applications, the collision operator $J(f)$ in (2.1) is typically of BGK-type

$$J(f) = -\frac{1}{\tau_v}(f - f^{\mathrm{eq}}). \tag{2.3}$$

The parameter $\tau_v > 0$ is called *relaxation time* and f^{eq} is the *equilibrium distribution*. In the isothermal case, f^{eq} depends on f through the variables ρ and $\mathbf{u}$ which are calculated according to (2.2), see for example [20,21,40]. For the standard D2Q9-model with nine velocities [36], we have

$$f^{\mathrm{eq}}[\rho,\mathbf{u}](\mathbf{v}) = \rho\left(1 + 3\mathbf{u}\cdot\mathbf{v} - \frac{3}{2}|\mathbf{u}|^2 + \frac{9}{2}(\mathbf{u}\cdot\mathbf{v})^2\right) f^*(\mathbf{v}), \tag{2.4}$$

where f^* is defined by

$$f^*(\mathbf{c}_i) = \begin{cases} \frac{4}{9}, & i = 0, \\ \frac{1}{9}, & i = 1,\ldots,4, \\ \frac{1}{36}, & i = 5,\ldots,8. \end{cases}$$

The equilibrium distribution is constructed in such a way that

$$\langle J(f)\rangle = 0 \quad \text{and} \quad \langle \mathbf{v}J(f)\rangle = 0,$$

which reflects conservation of mass and momentum in the collision process. The forcing term F is defined as

$$F = 3f^*(\mathbf{v})\mathbf{v}\cdot\mathbf{G},$$

where $\mathbf{G}$ is an external force acting per unit mass [18,25]. Since

$$\langle 1, f^*\rangle = 1, \quad \langle 1, \mathbf{v}_\alpha\mathbf{v}_\beta f^*\rangle = \frac{1}{3}\delta_{\alpha\beta}, \quad \langle 1, \mathbf{v}_\alpha\mathbf{v}_\beta\mathbf{v}_\gamma\mathbf{v}_\theta f^*\rangle = \frac{1}{9}(\delta_{\alpha\beta}\delta_{\gamma\theta} + \delta_{\alpha\gamma}\delta_{\beta\theta} + \delta_{\alpha\theta}\delta_{\beta\gamma}),$$

where $\delta_{\alpha\beta}$ denotes the Kronecker symbol. Hence, we obtain

$$\langle 1, 3f^*\mathbf{v}\cdot\mathbf{G}\rangle = 0 \quad \text{and} \quad \langle 1, 3f^*\mathbf{v}\mathbf{v}\mathbf{G}\rangle = 3\langle 1, f^*\mathbf{v}\mathbf{v}\rangle\mathbf{G} = \mathbf{G}.$$

In order to obtain a relation between the kinetic equation (2.1) and the incompressible Navier–Stokes equations, we introduce the *diffusive scaling* $\mathbf{x} \to \mathbf{x}/\epsilon$, $t \to t/\epsilon^2$ together with a rescaling of velocity $\mathbf{u} \to \epsilon\mathbf{u}$. This scaling describes the small Knudsen and low Mach number limit of kinetic equations, see [43,11,5,22] for details. Under these transformations, Eq. (2.1) is rewritten as

$$\frac{\partial f}{\partial t} + \frac{1}{\epsilon}\mathbf{v}\cdot\nabla f = -\frac{1}{\epsilon^2\tau_v}(f - f^{\mathrm{eq}}[\rho,\epsilon\mathbf{u}]) + \epsilon^2 F_\epsilon. \tag{2.5}$$

Notice that, in our case, Eq. (2.5) consists of nine equations for the occupation numbers $f_0,\ldots,f_8$. Here we also observe that a scaling $\epsilon^2 F_\epsilon$ has been used in order to obtain the correct source term in the incompressible limit as a consequence of the transformation into an equivalent set of moment equations in (2.6). In this case

$$F_\epsilon = 3f^*(\mathbf{v})\frac{\mathbf{v}}{\epsilon}\cdot\mathbf{G}.$$

We transform (2.5) into an equivalent set of moment equations (see also [27,14] for a similar approach) using moments based on the following $\mathbf{v}$-polynomials [17]:

$$\begin{aligned} &P_0(\mathbf{v}) = 1, \\ &P_1(\mathbf{v}) = \frac{v_1}{\epsilon}, \quad P_2(\mathbf{v}) = \frac{v_2}{\epsilon}, \\ &P_3(\mathbf{v}) = \frac{v_1^2}{\epsilon^2} - \frac{1}{3\epsilon^2}, \quad P_4(\mathbf{v}) = \frac{v_1 v_2}{\epsilon^2}, \quad P_5(\mathbf{v}) = \frac{v_2^2}{\epsilon^2} - \frac{1}{3\epsilon^2}, \\ &P_6(\mathbf{v}) = \frac{(3|\mathbf{v}|^2 - 4)v_1}{\epsilon^3}, \quad P_7(\mathbf{v}) = \frac{(3|\mathbf{v}|^2 - 4)v_2}{\epsilon^3}, \quad P_8(\mathbf{v}) = \frac{9|\mathbf{v}|^4 - 15|\mathbf{v}|^2 + 2}{\epsilon^4}. \end{aligned} \tag{2.6}$$

Note that $\langle P_0 f\rangle = \rho$, $\langle P_1 f\rangle = \rho u_1$ and $\langle P_2 f\rangle = \rho u_2$. The second order moments form a symmetric tensor

$$\boldsymbol{\Theta} = (\boldsymbol{\Theta}^x, \boldsymbol{\Theta}^y) = \begin{pmatrix} \theta_{11} & \theta_{12} \\ \theta_{12} & \theta_{22} \end{pmatrix} = \begin{pmatrix} \langle P_3 f\rangle & \langle P_4 f\rangle \\ \langle P_4 f\rangle & \langle P_5 f\rangle \end{pmatrix},$$

where $\boldsymbol{\Theta}^x = (\theta_{11}, \theta_{12})^{\mathrm{T}}$ and $\boldsymbol{\Theta}^y = (\theta_{12}, \theta_{22})^{\mathrm{T}}$. For the remaining moments we set

$$\mathbf{q} = \begin{pmatrix} q_1 \\ q_2 \end{pmatrix} = \begin{pmatrix} \langle P_6 f\rangle \\ \langle P_7 f\rangle \end{pmatrix}, \quad s = \langle P_8 f\rangle.$$

The equations of mass and momentum conservation are

$$\begin{aligned} &\partial_t \rho + \operatorname{div} \rho \mathbf{u} = 0, \\ &\partial_t \rho \mathbf{u} + \operatorname{div} \boldsymbol{\Theta} + \frac{1}{3\epsilon^2} \nabla \rho = \mathbf{G}. \end{aligned} \tag{2.7}$$

Here, the divergence is applied to the rows of $\boldsymbol{\Theta}$. The equation for $\boldsymbol{\Theta}$ is

$$\partial_t \boldsymbol{\Theta} + \frac{2}{3\epsilon^2} \mathbf{S}[\rho \mathbf{u}] + \frac{1}{3} \mathbf{Q}[\mathbf{q}] = -\frac{1}{\epsilon^2 \tau_v} (\boldsymbol{\Theta} - \rho \mathbf{u} \otimes \mathbf{u}), \tag{2.8}$$

where

$$\mathbf{S}[\mathbf{u}] = \frac{1}{2} \begin{pmatrix} 2\partial_x u_1 & \partial_y u_1 + \partial_x u_2 \\ \partial_y u_1 + \partial_x u_2 & 2\partial_y u_2 \end{pmatrix}, \quad \mathbf{Q}[\mathbf{q}] = \begin{pmatrix} \partial_y q_2 & \partial_y q_1 + \partial_x q_2 \\ \partial_y q_1 + \partial_x q_2 & \partial_x q_1 \end{pmatrix}.$$

Finally, the third and fourth order moments satisfy

$$\begin{aligned} &\partial_t \mathbf{q} + \frac{1}{\epsilon^2} \operatorname{div} \begin{pmatrix} \theta_{22} & 2\theta_{12} \\ 2\theta_{12} & \theta_{11} \end{pmatrix} + \frac{1}{6} \nabla s = -\frac{1}{\epsilon^2 \tau_v} \mathbf{q}, \\ &\partial_t s + \frac{4}{\epsilon^2} \operatorname{div} \mathbf{q} = -\frac{1}{\epsilon^2 \tau_v} s. \end{aligned} \tag{2.9}$$

Altogether, we obtain a hyperbolic system with stiff relaxation terms. Now we will demonstrate how the diffusion limit is obtained. From the momentum equation in (2.7) we conclude that $\nabla \rho$ tends to zero as $\epsilon \to 0$. Hence, ρ approaches a constant ρ_∞ (which is the Boussinesq relation in the isothermal case). Writing $\rho = \rho_\infty (1 + 3\epsilon^2 p)$, Eq. (2.7) transform into

$$\begin{aligned} &\partial_t p + \frac{1}{3\epsilon^2} \operatorname{div} \mathbf{u} = -\operatorname{div} p\mathbf{u}, \\ &\partial_t \mathbf{u} + \operatorname{div} \left(\frac{1}{\rho_\infty} \boldsymbol{\Theta} \right) + \nabla p = -3\epsilon^2 \partial_t (p\mathbf{u}) + \mathbf{G}. \end{aligned} \tag{2.10}$$

For $\epsilon \to 0$, Eq. (2.8) yields at the lowest order

$$\frac{1}{\rho_\infty} \boldsymbol{\Theta} = \mathbf{u} \otimes \mathbf{u} - \frac{2\tau_v}{3} \mathbf{S}[\mathbf{u}]. \tag{2.11}$$

Since the system (2.9) decouples completely from the other equations (in lowest order) and since $2\operatorname{div} \mathbf{S}[\mathbf{u}] = (\Delta + \nabla \operatorname{div}) \mathbf{u}$, we obtain from (2.10) and (2.11) the incompressible Navier–Stokes equations as a limiting system

$$\begin{aligned} &\operatorname{div} \mathbf{u} = 0, \\ &\partial_t \mathbf{u} + \operatorname{div} \mathbf{u} \otimes \mathbf{u} + \nabla p = \frac{\tau_v}{3} \Delta \mathbf{u} + \mathbf{G}, \end{aligned} \tag{2.12}$$

where the kinematic viscosity is related to the relaxation time by $\nu = \tau_v / 3$. We remark that Eqs. (2.7)–(2.9) can be viewed as a relaxation system for the incompressible Navier–Stokes equation (2.12).

2.2. Lattice-Boltzmann moment system for the energy equation

In this section, we present a derivation of the thermal energy equation based on a lattice-Boltzmann formulation [19,41]. We consider the case in which the temperature field is passively advected by fluid flow and obeys a simple passive scalar equation. Let R denote the gas constant, ρ, $\mathbf{u}$, and T the macroscopic density, velocity and temperature, respectively. An energy moment system for two-dimensional problems can be derived from

$$\rho R T = \left\langle P_0(\mathbf{v}) \frac{1}{2} f (\mathbf{v} - \mathbf{u})^2 \right\rangle.$$

A temperature distribution function can be defined as

$$g = \frac{(\mathbf{v}-\mathbf{u})^2}{2R} f$$

and the temperature is obtained from

$$\rho T = \langle P_0(\mathbf{v}) g \rangle. \tag{2.13}$$

An alternative formulation is presented in [18,42]. There, it was shown that for small Mach number flows, the discrete-velocity BGK model can be formulated using

$$\tilde{g} = \frac{g}{\rho}.$$

Using the transformed distribution we obtain the following equilibrium distribution function:

$$\tilde{g}^{\mathrm{eq}}[T,\rho,\mathbf{u}](\mathbf{v}) = T\left(1 + 3\mathbf{u}\cdot\mathbf{v} - \frac{3}{2}|\mathbf{u}|^2 + \frac{9}{2}(\mathbf{u}\cdot\mathbf{v})^2\right) f^*(\mathbf{v}), \tag{2.14}$$

where

$$T = \langle P_0(\mathbf{v})\tilde{g}\rangle.$$

We also denote $\langle P_1\tilde{g}\rangle = \Psi_1$, $\langle P_2\tilde{g}\rangle = \Psi_2$, $\langle P_1\tilde{g}^{\mathrm{eq}}\rangle = u_1 T$ and $\langle P_2\tilde{g}^{\mathrm{eq}}\rangle = u_2 T$, where

$$\tilde{g}^{\mathrm{eq}}[T,\rho,\mathbf{u}](\mathbf{v}) = T f^{\mathrm{eq}}[\rho,\mathbf{u}](\mathbf{v}),$$

with f^{eq} denoting the equilibrium function given by (2.4). In the subsequent discussion we replace $\tilde{g}$ by g. As usual the second-order moments form a symmetric tensor

$$\mathbf{\Pi} = (\mathbf{\Pi}^x, \mathbf{\Pi}^y) = \begin{pmatrix} \Pi_{11} & \Pi_{12} \\ \Pi_{12} & \Pi_{22} \end{pmatrix} = \begin{pmatrix} \langle P_3 g\rangle & \langle P_4 g\rangle \\ \langle P_4 g\rangle & \langle P_5 g\rangle \end{pmatrix},$$

where $\mathbf{\Pi}^x = (\Pi_{11}, \Pi_{12})^{\mathrm{T}}$ and $\mathbf{\Pi}^y = (\Pi_{12}, \Pi_{22})^{\mathrm{T}}$. For the remaining moments we set

$$\mathbf{q}_{\mathrm{c}} = \begin{pmatrix} q_{\mathrm{c}1} \\ q_{\mathrm{c}2} \end{pmatrix} = \begin{pmatrix} \langle P_6 g\rangle \\ \langle P_7 g\rangle \end{pmatrix}, \quad s_{\mathrm{c}} = \langle P_8 g\rangle.$$

The evolution equation is defined from Eq. (2.5) and for small Mach numbers and cases where compression does not take place and viscous heat dissipation effects are negligibly small we apply

$$\partial_t g + \frac{1}{\epsilon}\mathbf{v}\cdot\nabla g = -\frac{1}{\epsilon^2\tau_{\mathrm{c}}}(g - g^{\mathrm{eq}}[\rho,\epsilon\mathbf{u}]). \tag{2.15}$$

If there is a heat source term we extend the above equation similarly to Eq. (2.5). The thermal source term $\mathbf{Q}$ is defined using

$$q_\epsilon = 3 f^*(\mathbf{v})\frac{\mathbf{v}}{\epsilon}\cdot\mathbf{Q}. \tag{2.16}$$

The equation of the thermal distribution function can be written in the form

$$\partial_t g + \frac{1}{\epsilon}\mathbf{v}\cdot\nabla g = -\frac{1}{\epsilon^2\tau_{\mathrm{c}}}(g - g^{\mathrm{eq}}[\rho,\epsilon\mathbf{u}]) + q_\epsilon. \tag{2.17}$$

The relaxation system for the energy density and the energy flow can now be written as

$$\begin{aligned} &\partial_t T + \operatorname{div}\Psi = 0, \\ &\partial_t \Psi + \operatorname{div}\mathbf{\Pi} + \frac{1}{3\epsilon^2}\nabla T = -\frac{1}{\epsilon^2\tau_{\mathrm{c}}}(\Psi - \mathbf{u}T) + \frac{1}{\epsilon^2}\mathbf{Q}. \end{aligned} \tag{2.18}$$

Taking higher-order moments completes the system. The details will be skipped but we would like to note that the remaining moment equations decouple from the ones derived above. The lowest-order term in the limit as $\epsilon \to 0$ gives the following equation:

$$\begin{aligned} &\partial_t T + \operatorname{div} \Psi = 0, \\ &\Psi = -\frac{\tau_c}{3}\nabla T + \mathbf{u}T + \frac{\tau_c}{3}\mathbf{Q}, \end{aligned} \tag{2.19}$$

or simply

$$\partial_t T + \operatorname{div}\left(\mathbf{u}T - \frac{\tau_c}{3}\nabla T + \frac{\tau_c}{3}\mathbf{Q}\right) = 0, \tag{2.20}$$

where the thermal diffusion coefficient is now $\kappa = \tau_c/3$. We also note that in this case the source term q_ϵ in (2.17) provides an extra flux in the energy equation in the limit.

2.3. Simplified relaxation systems

Now we are in a position to derive a relaxation system that will be used in our numerical schemes in the next section. We consider the system of equations in (2.8) and (2.10) with $\rho_\infty \equiv 1$. We would like to simplify the system in such a way that the same limit for lower order terms as the original system, (2.8) and (2.10), is preserved. Next, from Eq. (2.10) we neglect the term $-\operatorname{div} p\mathbf{u}$ and $-3\epsilon^2\partial_t p\mathbf{u}$. From Eq. (2.8) we neglect the term $\frac{1}{3}\mathbf{Q}[\mathbf{q}]$ and introduce a new term, $\nabla^{\mathbf{a}}[\mathbf{u}]$, as follows:

For p, $\mathbf{u}$ and $\boldsymbol{\Theta}$ as defined above, we consider the system

$$\begin{aligned} &\partial_t p + \frac{1}{\epsilon^2}\operatorname{div}\mathbf{u} = 0, \\ &\partial_t \mathbf{u} + \operatorname{div}\boldsymbol{\Theta} + \nabla p = \mathbf{G}, \\ &\partial_t \boldsymbol{\Theta} + \nabla^{\mathbf{a}}[\mathbf{u}] + 2\mathbf{S}^\epsilon[\mathbf{u}] = -\frac{1}{\epsilon^2\tau_v}(\boldsymbol{\Theta} - \mathbf{u}\otimes\mathbf{u}), \quad \partial_t T + \operatorname{div}\Psi = 0, \\ &\partial_t \Psi + \operatorname{div}\boldsymbol{\Pi}_{\mathbf{b}} + \frac{1}{\epsilon^2}\nabla T = -\frac{1}{\epsilon^2\tau_c}(\Psi - \mathbf{u}T) + \frac{1}{\epsilon^2}\mathbf{Q}, \end{aligned} \tag{2.21}$$

where

$$\mathbf{S}^\epsilon[\mathbf{u}] = \mathbf{S}[\mathbf{u}] - \frac{\epsilon^2}{2}\nabla^{\mathbf{a}}[\mathbf{u}].$$

We have added and subtracted the term

$$\nabla^{\mathbf{a}}[\mathbf{u}] = (a_1^2\partial_x\mathbf{u}, a_2^2\partial_y\mathbf{u}) = \begin{pmatrix} a_1^2\partial_x u_1 & a_2^2\partial_y u_1 \\ a_1^2\partial_x u_2 & a_2^2\partial_y u_2 \end{pmatrix},$$

where $a_1^2\partial_x\mathbf{u} = (a_1^2\partial_x u_1, a_1^2\partial_x u_2)^{\mathrm{T}}$ and $a_2^2\partial_y\mathbf{u} = (a_2^2\partial_y u_1, a_2^2\partial_y u_2)^{\mathrm{T}}$ with $\mathbf{a} = (a_1, a_2)^{\mathrm{T}} \in \mathbb{R}^2_+$. In addition we have replaced $\boldsymbol{\Pi}$ by

$$\boldsymbol{\Pi}_{\mathbf{b}} = \begin{pmatrix} b_1^2 T & 0 \\ 0 & b_2^2 T \end{pmatrix},$$

where $\mathbf{b} = (b_1, b_2)^{\mathrm{T}} \in \mathbb{R}^2_+$. Obviously the limit equations for this system are again the coupled equation (2.21) with kinematic viscosity $\nu = \tau_v$ and heat diffusion coefficient $\kappa = \tau_c$.

Remark 1. Considering the nonstiff advection parts in (2.21) separately for $\mathbf{u}$, $\boldsymbol{\Theta}$, T and Ψ we obtain a hyperbolic system with characteristic speeds $\pm a_1$, $\pm b_1$ in the x-direction and $\pm a_2$, $\pm b_2$ in the y-direction

$$\begin{aligned} &\partial_t \mathbf{u} + \operatorname{div}\boldsymbol{\Theta} = \mathbf{G}, \\ &\partial_t \boldsymbol{\Theta} + \nabla^{\mathbf{a}}[\mathbf{u}] = 0, \\ &\partial_t T + \operatorname{div}\Psi = 0, \\ &\partial_t \Psi + \operatorname{div}\boldsymbol{\Pi}_{\mathbf{b}} = 0. \end{aligned} \tag{2.22}$$

As we will see in Section 3, $\mathbf{a}$ and $\mathbf{b}$ are chosen depending on the local characteristic speeds.

Clearly, one can develop another class of relaxation systems by letting the first equation in Eq. (2.21) relax to its limit in lowest order terms as $\epsilon \to 0$ without altering the others. This is practical if one considers an implementation in the vorticity-stream function formulation, compare [3] for a similar formulation in the isothermal case.

2.4. Coupled convection–radiation systems

We consider flow problems in participating grey media that interact with radiative transfer through emission, absorption and scattering. This means the source term in the flow equations contains a radiative heat flux which we denote by $\mathbf{Q}_R$. Let $I(t, \mathbf{x}, \omega)$ be the radiative intensity at position $\mathbf{x}$, time t, traveling in direction ω with speed c. Then, the isotropic radiative transfer equation is given by [33,32]

$$\frac{1}{c}\partial_t I + \omega \cdot \nabla I = \sigma_s\left(\frac{1}{4\pi}\int_{S^2} I \,\mathrm{d}\omega - I\right) + \sigma_a(B(T) - I), \tag{2.23}$$

where σ_s and σ_a are the scattering and absorption coefficients, respectively, which may depend on space $\mathbf{x}$. The integral in (2.23) is taken over all directions in the unit sphere S^2. The function $B(T)$ is the grey Planck's function which defines a nonlinear relationship between the participating medium and its temperature, and it is defined as

$$B(T) = \sigma_B T^4, \tag{2.24}$$

where σ_B is the Stefan–Boltzmann constant [32]. Note that in the above coupling we have assumed a thermodynamic equilibrium such that the fluid temperature and the radiation temperature are equal. Since the photons travel with the speed of light, the term $1/c$ in (2.23) is negligible and is dropped in our computations. The radiative heat flux $\mathbf{Q}_R$ is defined by

$$\mathbf{Q}_R = \int_{S^2} I\omega \,\mathrm{d}\omega. \tag{2.25}$$

Hence, integrating Eq. (2.23) over the whole solid angle $\omega \in S^2$ yields a relation for the radiative heat source

$$\nabla \cdot \mathbf{Q}_R = \int_{S^2} \sigma_a(B(T) - I)\,\mathrm{d}\omega, \tag{2.26}$$

which is substituted in the energy equation (2.20). The term $\tau_c/3$ is incorporated into σ_a. In the models considered here we assume flow in the low Mach number limit. For such flows there is a linear relationship between density and temperature defined as

$$\rho(T) = \rho_\infty(1 - \beta(T - T_\infty)),$$

where β is the coefficient of thermal expansion, ρ_∞ and T_∞ are reference density and reference temperature, respectively. The system of equations takes the form

$$\begin{aligned}
&\operatorname{div}\mathbf{u} = 0,\\
&\partial_t \mathbf{u} + \operatorname{div}\mathbf{u}\otimes\mathbf{u} + \nabla p = \nu\Delta\mathbf{u} + \mathbf{G},\\
&\partial_t T + \operatorname{div}(\mathbf{u}T) = \kappa\Delta T - \nabla\cdot\mathbf{Q}_R,\\
&\omega\cdot\nabla I + (\sigma_a + \sigma_s)I = \frac{\sigma_s}{4\pi}\int_{S^2} I\,\mathrm{d}\omega + \sigma_a B(T),
\end{aligned} \tag{2.27}$$

where $\mathbf{G} = \rho\mathbf{g}$, $\mathbf{g}$ is the gravitational force and $\nabla\cdot\mathbf{Q}_R$ is given by (2.26).

Remark 2. Some remarks are in order:

(i) In the microscopic setting we include the radiative heat transfer as a source term while the asymptotic derivations realize it as an extra flux term.

(ii) It is well known that the radiative transfer is a non-local phenomenon; photons which are the main medium of transfer do not need a medium in order to propagate; and the temperature dependence of radiation is nonlinear. Conduction and convection have a linear temperature dependence (Fourier's law). Therefore, it makes sense to treat the radiative term as a source in the microscopic scale.
(iii) In addition, whether radiation is a minor or dominant mode of heat transfer depends on the temperature and the nature of the material.

For the computational examples, we consider a case of free convection and a case of forced convection. In particular we present dimensionless forms of the fluid and energy flow equations in a grey participating medium.

3. Numerical schemes

To develop numerical schemes for the relaxation systems developed in Section 2.3, we will consider Eq. (2.21). In the next subsection we will discuss a derivation for a numerical procedure applied to flow equations. Thereafter a numerical approach for radiative transfer is presented.

3.1. Solution procedure for flow equations

In this section, high-order upwind discretizations are developed for the non-stiff advection part in the relaxation system (2.21). The stiff part is treated by high-order centered differences, as in [3]. In the remainder of this section the time continuous version of the scheme is considered (method of lines). We also point out that the non-stiff parts from momentum and energy transport equations are completely decoupled. Hence, they are treated separately in the ensuing discussion.

To discretize the equations in space we use, for the sake of simplicity, a uniform grid in x and y with gridpoints (x_i, y_j) and spacing $\Delta x = \Delta y = h$. Consider the non-stiff linear part of the system (2.21) as presented in (2.22). One observes that for the x-direction, $\mathbf{\Theta}^x \pm a_1\mathbf{u}$ and $\Psi_1 \pm b_1 T$ are the characteristic variables associated with the characteristic speeds $\pm a_1$ and $\pm b_1$, respectively. For the y-direction the characteristic variables associated with the characteristic speeds $\pm a_2$ and $\pm b_2$ are $\mathbf{\Theta}^y \pm a_2\mathbf{u}$ and $\Psi_2 \pm b_2 T$, respectively. According to these considerations the values of the characteristic variables are determined at cell-boundaries following the approach in [24]. This can be done in a straightforward way for a second-order method. For a third-order method we use for the reconstruction step a third-order CWENO interpolant, see for example [35,30] and further references therein. Similar reconstructions were also applied in [3,2,38]. We report for the convenience of the reader the polynomials for the two-dimensional reconstruction in the x-direction. These polynomials at the gridpoint (x_i, y_j) are constructed as

$$\mathbf{p}_{ij}(\mathbf{z}; x) = \mathbf{z}_{ij} + \mathbf{s}_{ij}(x - x_i), \tag{3.1}$$

where the MinMod limiter

$$\mathbf{s}_{ij}(\mathbf{z}) = \frac{1}{h}\mathrm{MinMod}(\mathbf{z}_{ij} - \mathbf{z}_{i-1j}, \mathbf{z}_{i+1j} - \mathbf{z}_{ij}),$$

for the second-order MUSCL case and as

$$\mathbf{p}_{ij}(\mathbf{z}; x) = w_{\mathrm{L}}\mathbf{P}^{\mathrm{L}}_{ij}(\mathbf{z}; x) + w_{\mathrm{R}}\mathbf{P}^{\mathrm{R}}_{ij}(\mathbf{z}; x) + w_{\mathrm{C}}\mathbf{P}^{\mathrm{C}}_{ij}(\mathbf{z}; x) \tag{3.2}$$

with

$$\mathbf{P}^{\mathrm{R}}_{ij}(\mathbf{z}; x) = \mathbf{z}_{ij} + \frac{1}{h}(\mathbf{z}_{i+1j} - \mathbf{z}_{ij})(x - x_i), \quad \mathbf{P}^{\mathrm{L}}_{ij}(\mathbf{z}; x) = \mathbf{z}_{ij} + \frac{1}{h}(\mathbf{z}_{ij} - \mathbf{z}_{i-1j})(x - x_i),$$

$$\mathbf{P}^{\mathrm{C}}_{ij}(\mathbf{z}; x) = \mathbf{z}_{ij} - \frac{1}{12}(\mathbf{z}_{i+1j} - 2\mathbf{z}_{ij} + \mathbf{z}_{i-1j}) - \frac{1}{12}(\mathbf{z}_{ij+1} - 2\mathbf{z}_{ij} + \mathbf{z}_{ij-1}) + \frac{1}{2h}(\mathbf{z}_{i+1j} - \mathbf{z}_{i-1j})(x - x_i)$$
$$+ \frac{1}{h^2}(\mathbf{z}_{i+1j} - 2\mathbf{z}_{ij} + \mathbf{z}_{i-1j})(x - x_i)^2.$$

for the third-order CWENO case. The nonlinear CWENO weights w_k, $k = \mathrm{L}, \mathrm{R}, \mathrm{C}$ in (3.2) are given as

$$w_k = \frac{\alpha_k}{\sum_l \alpha_l}, \quad \alpha_k = \frac{c_k}{(\gamma + \mathrm{IS}_k)^\beta}, \quad c_\mathrm{L} = \frac{1}{4}, \quad c_\mathrm{R} = \frac{1}{4}, \quad c_\mathrm{C} = \frac{1}{2},$$

with $\gamma = 10^{-6}$ and $\beta = 2$. The smoothness indicators IS_k, $k = \mathrm{L}, \mathrm{R}, \mathrm{C}$ are defined by

$$\mathrm{IS}_\mathrm{L} = (v_{ij} - v_{i-1j})^2, \quad \mathrm{IS}_\mathrm{R} = (v_{i+1j} - v_{ij})^2, \quad \mathrm{IS}_\mathrm{C} = \frac{13}{3}(v_{i+1j} - 2v_{ij} + v_{i-1j})^2 + \frac{1}{4}(v_{i+1j} - v_{i-1j})^2.$$

Clearly any other high-order reconstruction procedure applies. To determine the characteristic variables at the boundary of the cells $[x_{i-1/2}, x_{i+1/2}] \times [y_{j-1/2}, y_{j+1/2}]$ we apply

$$\begin{aligned}
&(\boldsymbol{\Theta}^x + a_1\mathbf{u})_{i+1/2j} = \mathbf{p}_{ij}(\boldsymbol{\Theta}^x + a_1\mathbf{u}; x_{i+1/2}), \quad (\boldsymbol{\Theta}^x - a_1\mathbf{u})_{i+1/2j} = \mathbf{p}_{i+1j}(\boldsymbol{\Theta}^x - a_1\mathbf{u}; x_{i+1/2}),\\
&(\Psi_1 + b_1 T)_{i+1/2j} = \mathbf{p}_{ij}(\Psi_1 + b_1 T; x_{i+1/2}), \quad (\Psi_1 - b_1 T)_{i+1/2j} = \mathbf{p}_{i+1j}(\Psi_1 - b_1 T; x_{i+1/2}).
\end{aligned} \tag{3.3}$$

An analogous procedure is used for the y-direction by considering the characteristic variables $(\boldsymbol{\Theta}^y \pm a_2\mathbf{u})_{ij+1/2}$ and $(\Psi_2 \pm b_2 T)_{ij+1/2}$. We denote by $\mathbf{F}_h^{(1)}$, $\mathbf{F}_h^{(2)}$, $F_h^{(3)}$, and $\mathbf{F}_h^{(4)}$ the discretization of the convective parts in Eq. (2.21) $\mathrm{div}\boldsymbol{\Theta}$, $\nabla^{\mathbf{a}}[\mathbf{u}]$, $\mathrm{div}\Psi$, and $\mathrm{div}\boldsymbol{\Pi}_\mathrm{b}$, respectively. Using the reconstruction polynomial given above componentwise one obtains

$$\begin{aligned}
\mathbf{F}_h^{(1)}(\boldsymbol{\Theta}, \mathbf{u}) &= \frac{1}{h}\left(\boldsymbol{\Theta}^x_{i+1/2j} - \boldsymbol{\Theta}^x_{i-1/2j}\right) + \frac{1}{h}\left(\boldsymbol{\Theta}^y_{ij+1/2} - \boldsymbol{\Theta}^y_{ij-1/2}\right),\\
\mathbf{F}_h^{(2)}(\boldsymbol{\Theta}, \mathbf{u}) &= \left(\frac{a_1^2}{h}(\mathbf{u}_{i+1/2,j} - \mathbf{u}_{i-1/2j}), \frac{a_2^2}{h}(\mathbf{u}_{ij+1/2} - \mathbf{u}_{ij-1/2})\right)^\mathrm{T},\\
\mathbf{F}_h^{(3)}(\Psi, T) &= \frac{1}{h}(\Psi_{1i+1/2j} - \Psi_{1i-1/2j}) + \frac{1}{h}(\Psi_{2ij+1/2} - \Psi_{2ij-1/2}),\\
\mathbf{F}_h^{(4)}(\Psi, T) &= \left(\frac{b_1^2}{h}(T_{i+1/2,j} - b_1^2 T_{i-1/2j}), \frac{b_2^2}{h}(T_{ij+1/2} - T_{ij-1/2})\right)^\mathrm{T},
\end{aligned}$$

where the numerical fluxes are given by

$$\begin{aligned}
\boldsymbol{\Theta}^x_{i+1/2j} &= \frac{1}{2}\left((\boldsymbol{\Theta}^x + a_1\mathbf{u})_{i+1/2j} + (\boldsymbol{\Theta}^x - a_1\mathbf{u})_{i+1/2j}\right),\\
\mathbf{u}_{i+1/2j} &= \frac{1}{2a_1}\left((\boldsymbol{\Theta}^x + a_1\mathbf{u})_{i+1/2j} - (\boldsymbol{\Theta}^x - a_1\mathbf{u})_{i+1/2j}\right),\\
\Psi_{1i+1/2j} &= \frac{1}{2}\left((\Psi_1 + b_1 T)_{i+1/2j} + (\Psi_1 - b_1 T)_{i+1/2j}\right),\\
T_{i+1/2j} &= \frac{1}{2b_1}\left((\Psi_1 + b_1 T)_{i+1/2j} - (\Psi_1 - b_1 T)_{i+1/2j}\right),
\end{aligned}$$

where the terms on the right-hand side are defined by the interpolants in (3.3). For more details we refer to [3].

To discretize the pressure variable and the stiff parts i.e., terms with the coefficient $\frac{1}{\epsilon^2}$ in Eq. (2.21), firstly, we denote the discrete gradient by $\mathbf{G}_h$ and the discrete divergence by $\mathbf{D}_h$. They are given by second- or fourth-order centered differences for second-order or third-order approaches, respectively. $\mathbf{S}_h^\epsilon$ and $\mathbf{S}_h$ denote second- or fourth-order centered difference approximations of $\mathbf{S}^\epsilon$ and $\mathbf{S}$, respectively. Finally, we obtain a high-order spatial discretization for the moment system characterized by

$$\begin{aligned}
&\dot{p} + \frac{1}{\epsilon^2}\mathbf{D}_h \cdot \mathbf{u} = 0,\\
&\dot{\mathbf{u}} + \mathbf{F}_h^{(1)}(\boldsymbol{\Theta}, \mathbf{u}) + \mathbf{G}_h p = \mathbf{G},\\
&\dot{\boldsymbol{\Theta}} + \mathbf{F}_h^{(2)}(\boldsymbol{\Theta}, \mathbf{u}) + \frac{2}{\epsilon^2}\mathbf{S}_h^\epsilon(\mathbf{u}) = -\frac{1}{\epsilon^2\tau_v}(\boldsymbol{\Theta} - \mathbf{u}\otimes\mathbf{u}),\\
&\dot{T} + \mathbf{F}_h^{(3)}(\Psi, T) = 0,\\
&\dot{\Psi} + \mathbf{F}_h^{(4)}(\Psi, T) + \frac{1}{\epsilon^2}G_h T = -\frac{1}{\epsilon^2\tau_\mathrm{c}}(\Psi - \mathbf{u}T) + \frac{1}{\epsilon^2}\mathbf{Q},
\end{aligned} \tag{3.4}$$

or equivalently

$$\begin{aligned}
&\mathbf{D}_h \cdot \mathbf{G}_h p - 2\epsilon^2 \ddot{p} = -\mathbf{D}_h \cdot \mathbf{F}_h^{(1)}(\boldsymbol{\Theta}, \mathbf{u}),\\
&\dot{\mathbf{u}} + \mathbf{F}_h^{(1)}(\boldsymbol{\Theta}, \mathbf{u}) + \mathbf{G}_h p = \mathbf{G},\\
&\dot{\boldsymbol{\Theta}} + \mathbf{F}_h^{(2)}(\boldsymbol{\Theta}, \mathbf{u}) = -\frac{1}{\epsilon^2 \tau_v}(\boldsymbol{\Theta} - \mathbf{u} \otimes \mathbf{u} + 2\tau_v \mathbf{S}_h^{\epsilon}(\mathbf{u})),\\
&\dot{T} + \mathbf{F}_h^{(3)}(\Psi, T) = 0,\\
&\dot{\Psi} + \mathbf{F}_h^{(4)}(\Psi, T) = -\frac{1}{\epsilon^2 \tau_c}(\Psi - \mathbf{u}T + \tau_c \mathbf{G}_h T - \tau_c \mathbf{Q}).
\end{aligned}$$

A corresponding high-order upwind-based space discretization for the relaxed incompressible Navier–Stokes/Boussinesq equations is obtained considering the limit of the above discretization as $\epsilon \to 0$

$$\begin{aligned}
&\mathbf{D}_h \cdot \mathbf{G}_h p = -\mathbf{D}_h \cdot \mathbf{F}_h^{(1)}(\mathbf{u}),\\
&\dot{\mathbf{u}} = -\mathbf{F}_h^{(1)}(\mathbf{u} \otimes \mathbf{u} - 2\tau_v \mathbf{S}_h(\mathbf{u}), \mathbf{u}) - \mathbf{G}_h p + \mathbf{G},\\
&\dot{T} = -\mathbf{F}_h^{(3)}(\mathbf{u}T - \tau_c G_h T + \tau_c \mathbf{Q}, T).
\end{aligned}$$

Remark 3. To treat only the limit equations ($\epsilon = 0$) we could use any explicit high order Runge–Kutta method combined with a Poisson solver and the limiting (relaxed) spatial discretization. The Poisson equation is in this case only used to determine the divergence-free velocities via ∇p and not to advance the pressure for one time step.

Let us denote the time step by Δt and use superscript n to denote the time iterations. We treat the non-stiff parts explicitly and the stiff parts implicitly. We demonstrate the application of this approach using a first-order scheme. For the first-order IMEX method we can use the following simple time discretization:

$$\begin{aligned}
&\mathbf{u}^{n+1} = \mathbf{u}^n - \Delta t(\operatorname{div} \boldsymbol{\Theta}^n + \nabla p^{n+1}) + \Delta t \mathbf{G}^n,\\
&\boldsymbol{\Theta}^{n+1} = \boldsymbol{\Theta}^n - \Delta t \nabla^{\mathbf{a}}[\mathbf{u}^n] - \frac{\Delta t}{\epsilon^2 \tau_v}(\boldsymbol{\Theta}^{n+1} + 2\tau \mathbf{S}^{\epsilon}[\mathbf{u}^{n+1}] - \mathbf{u}^{n+1} \otimes \mathbf{u}^{n+1}),\\
&T^{n+1} = T^n - \Delta t \operatorname{div} \Psi^n,\\
&\Psi^{n+1} = \Psi^n - \Delta t \operatorname{div} \boldsymbol{\Pi}_b^n - \frac{\Delta t}{\epsilon^2 \tau_c}(\Psi^{n+1} - \mathbf{u}^{n+1} T^{n+1} + \tau_c \mathbf{G}_h T^{n+1} - \tau_c \mathbf{Q}^{n+1}),\\
&p^{n+1} = p^n - \frac{\Delta t}{\epsilon^2} \operatorname{div} \mathbf{u}^{n+1}.
\end{aligned} \tag{3.5}$$

Substituting the last equation in (3.5) into the first equation in (3.5) yields a Helmholtz equation for the pressure

$$\Delta p^{n+1} - \frac{\epsilon^2}{\Delta t^2} p^{n+1} = \frac{1}{\Delta t} \operatorname{div} \mathbf{u}^n - \operatorname{div}(\operatorname{div} \boldsymbol{\Theta}^n) - \frac{\epsilon^2}{\Delta t^2} p^n. \tag{3.6}$$

This equation can be solved by a suitable iterative method. The velocity, $\mathbf{u}^{n+1}$, is determined using the first equation in (3.5). Obviously, as $\epsilon \to 0$ the time marching tends to a time discretization of the thermal incompressible Navier–Stokes equations. We obtain for $\epsilon \to 0$ the Poisson equation for the pressure

$$\Delta p^{n+1} = \frac{1}{\Delta t} \operatorname{div} \mathbf{u}^n - \operatorname{div}(\operatorname{div} \boldsymbol{\Theta}^n),$$

together with

$$\begin{aligned}
&\mathbf{u}^{n+1} = \mathbf{u}^n - \Delta t(\operatorname{div} \boldsymbol{\Theta}^n + \nabla p^{n+1}) + \Delta t \mathbf{G}^n,\\
&\boldsymbol{\Theta}^{n+1} = 2\tau_v \mathbf{S}[\mathbf{u}^{n+1}] - \mathbf{u}^{n+1} \otimes \mathbf{u}^{n+1},\\
&T^{n+1} = T^n - \Delta t \operatorname{div} \Psi^n,\\
&\Psi^{n+1} = \mathbf{u}^{n+1} T^{n+1} - \tau_c \mathbf{G}_h T^{n+1} + \tau_c \mathbf{Q}^{n+1}.
\end{aligned}$$

Thus, in the limit, we have obtained the usual projection method for the incompressible Navier–Stokes/Boussinesq equations. We note that the incompressibility condition is fulfilled for the velocity field **u** at every time step. In the IMEX notation the above first-order scheme is given by the explicit and implicit *Butcher tableau*

$$\begin{array}{c|cc} 0 & 0 & 0 \\ 1 & 0 & 1 \\ \hline & 0 & 1 \end{array} \qquad \begin{array}{c|cc} 0 & 0 & 0 \\ 1 & 1 & 0 \\ \hline & 1 & 0 \end{array}$$

For the above semi-implicit time discretization the usual hyperbolic and parabolic CFL conditions have to be fulfilled to guarantee stability. For the third-order time discretization we choose a two stage IMEX Runge Kutta method [34]. Its associated explicit and implicit *Butcher tableau* are

$$\begin{array}{c|ccc} 0 & 0 & 0 & 0 \\ \gamma & \gamma & 0 & 0 \\ 1-\gamma & \gamma-1 & 2-2\gamma & 0 \\ \hline & 0 & \frac{1}{2} & \frac{1}{2} \end{array} \qquad \begin{array}{c|ccc} 0 & 0 & 0 & 0 \\ \gamma & 0 & \gamma & 0 \\ 1-\gamma & 0 & 1-2\gamma & \gamma \\ \hline & 0 & \frac{1}{2} & \frac{1}{2} \end{array}$$

where $\gamma = \frac{3+\sqrt{3}}{6}$. Its formulation can be performed as in (3.5) and details are omitted. Other IMEX schemes of third and higher order are also discussed in [34].

3.2. Solution procedure for radiative transfer

The radiative transfer equation (2.23) can be solved using any existing code from computational radiative transfer such as Monte Carlo or discrete-ordinates methods. The later method is selected to be used in the present work mainly because the Monte Carlo methods are computationally very demanding. Other fast solvers as those recently developed in [39,37] can also be used. Here, the angle and space variables are discretized using discrete-ordinates and finite volume methods. The outstanding aspect of discrete-ordinates method is that such an integral is approximated by a procedure with low computational cost, which is analogous to the Gauss–Legendre method. It consists of the substitution of the integral term in the radiative transfer equation (2.23) with a weighted summation of the integrand at selected ordinates of the unit sphere. This method is sometimes referred to as the S_N approximation, where N represents the number of discrete values of direction cosines to be considered. In general, the total number of ordinate directions M in a set S_N is given by $M = N(N+2)/2$.

The S_8 discretization is well designed for solving radiative transfer problems. For each direction ω_m of the quadrature, a specific weight w_m is associated with a set of three cosine angles μ_m, ξ_m and η_m in direct Cartesian grid (x, y, z). The cosine angles and the weights for S_8 quadrature are listed in Table 1. Other discrete S_N sets from [33,15] are also applicable. For the two-dimensional Cartesian coordinates, the radiative transfer equation (2.23) can be expressed for each individual ordinate direction, m, as

$$\mu_m \partial_x I_m + \xi_m \partial_y I_m + (\sigma_a + \sigma_s) I_m = \frac{\sigma_s}{4\pi} \sum_{k=1}^{M} w_k I_k + \sigma_a B(T), \quad m = 1, 2, \ldots, M, \tag{3.7}$$

where I_m denotes the radiative intensity at the discrete ordinate ω_m. Next, the finite volume technique is applied, which consists of the integration of the S_N-equation (3.7) over a control volume. The result is an equation relating the value of an arbitrary function ψ at the nodal point, $\psi_{i+1/2j+1/2}$, to the value at each adjacent line ψ_{ij}, ψ_{i+1j}, ψ_{ij+1} and ψ_{i+1j+1}. The fully discrete problem corresponding to Eq. (2.23) is written as

$$\begin{aligned} &\mu_m \frac{I_{m,i+1j} - I_{m,ij}}{\Delta x} + \xi_m \frac{I_{m,ij+1} - I_{m,ij}}{\Delta y} + (\sigma_{a_{i+1/2j+1/2}} + \sigma_{s_{i+1/2j+1/2}}) I_{m,i+1/2j+1/2} \\ &\quad = \frac{\sigma_{s_{i+1/2j+1/2}}}{4\pi} \sum_{k=1}^{M} w_k I_{k,i+1/2j+1/2} + \sigma_{a_{i+1/2j+1/2}} B_{i+1/2j+1/2}(T), \end{aligned} \tag{3.8}$$

Table 1
Discrete ordinates and quadrature weights for the S_8 set (one octant only)

m	μ_m	ξ_m	η_m	w_m
1	0.97097459	0.16912768	0.16912768	0.14613894
2	0.79878814	0.16912768	0.57735027	0.15983890
3	0.79878814	0.57735027	0.16912768	0.15983890
4	0.57735027	0.16912768	0.79878814	0.15983890
5	0.57735027	0.57735027	0.57735027	0.17334611
6	0.57735027	0.79878814	0.16912768	0.15983890
7	0.16912768	0.16912768	0.97097459	0.14613894
8	0.16912768	0.57735027	0.79878814	0.15983890
9	0.16912768	0.79878814	0.57735027	0.15983890
10	0.16912768	0.97097459	0.16912768	0.14613894

where the cell averages of a function ψ are given by

$$\psi_{i+1j} = \frac{1}{\Delta y}\int_{y_j}^{y_{j+1}} \psi(x_i, y)\,\mathrm{d}y, \quad \psi_{ij+1} = \frac{1}{\Delta x}\int_{x_i}^{x_{i+1}} \psi(x, y_j)\,\mathrm{d}x, \quad \psi_{ij} = \frac{1}{\Delta x \Delta y}\int_{x_i}^{x_{i+1}}\int_{y_j}^{y_{j+1}} \psi(x, y)\,\mathrm{d}x\,\mathrm{d}y, \tag{3.9}$$

The cell center and cell boundary function in fluxes (3.9) are related to each other by a selected interpolation scheme. Here, we use the diamond difference method which consists of approximating the function values at the cell centers by the average of their values at the neighboring nodes. Thus, the function value of $\psi_{i+1/2j+1/2}$ at the cell center is simply approximated by bilinear interpolation as

$$\psi_{i+1/2j+1/2} = \frac{\psi_{ij} + \psi_{i+ij} + \psi_{ij+1} + \psi_{i+1j+1}}{4}. \tag{3.10}$$

With the introduction of the above interpolation relations into (3.8), the resulting fully discrete equations can be solved by proceeding in the direction of photon travel on the spatial mesh, that is, sweeping away from the boundary conditions in the mesh. For problems involving scattering media or reflecting boundaries, the discrete-ordinates equations are coupled and therefore have to be solved iteratively. In the current work, to solve the discretized equation (3.8), we first eliminate the intensity from the resulting discretized equation (3.8) then a linear system of the form

$$(\mathbf{I} - \mathbf{A})\boldsymbol{\phi} = \mathbf{f}, \tag{3.11}$$

has to be solved for the mean intensity ϕ

$$\phi_{ij} = \sum_{k=1}^{M} w_k I_{k,ij}.$$

The Schur matrix $\mathbf{A}$ contains the discretized transport and integral operators from (3.8), $\mathbf{f}$ the right-hand side and $\mathbf{I}$ is the identity matrix, see [39] for a detailed matrix formulation of (3.11). In order to construct the matrix $\mathbf{A}$ in (3.11), one has to use a Gaussian elimination known in computational radiative transfer as sweeping procedure. All the results given throughout this paper were obtained using the diffusion-synthetic acceleration (DSA) method. The DSA method uses the diffusion approach as preconditioner for the source iteration applied to the linear system (3.11). For a detailed formulation of this algorithm we refer the reader to [39].

4. Results and discussions

In order to study the performance of the proposed numerical models, two test examples have been computed herein for natural and forced convection–radiation flows. The aim was to show that, for small relaxation rates, the discrete-velocity relaxation models reproduce the corresponding flow patterns, and also to show that the high-order relaxation schemes accurately capture the flow structures with very little numerical diffusion, even after long time simulations. All the results presented in this section are computed with variable time steps Δt adjusted at each step by

$$\Delta t = Cr \cdot \min\left(\frac{\Delta x}{|a_{i\pm 1/2j}|}, \frac{\Delta y}{|b_{ij\pm 1/2}|}\right), \tag{4.1}$$

where $a_{i\pm 1/2j}$ and $b_{ij\pm 1/2}$ are the characteristic speeds in the relaxation system selected locally in each grid cell $[x_{i-1/2}, x_{i+1/2}] \times [y_{j-1/2}, y_{j+1/2}]$ as

$$a_{i+1/2j} = 2\max\left\{|p_{ij}(u_1; x_{i+1/2})|, |p_{i+1j}(u_1; x_{i+1/2})|\right\},$$
$$b_{ij+1/2} = 2\max\left\{|p_{ij}(u_2; y_{j+1/2})|, |p_{ij+1}(u_2; y_{j+1/2})|\right\}.$$

The other characteristic speeds $a_{i-1/2j}$ and $b_{ij-1/2}$ are calculated analogously. Here, the polynomials p_{ij} are defined for scalar variables u_1 and u_2 analogous to the definition in (3.1) for second-order method or in (3.2) for the third-order method. In (4.1), Cr is the Courant number set to 0.8 for all test cases to ensure stability. The time integration process is stopped if

$$\frac{|\phi_{ij}^{n+1} - \phi_{ij}^{n}|}{\max|\phi_{ij}^{n+1}|} \leqslant 10^{-6}, \tag{4.2}$$

where ϕ represents u, v or T. In our computations the relaxation rate $\epsilon = 10^{-10}$ and all the linear systems of algebraic equations are solved using a preconditioned conjugate gradient solver with a stopping criteria set to 10^{-6}.

4.1. Natural convection–radiation

We consider the well-established problem of natural convection in a squared cavity subject to an horizontal temperature difference (applied at the walls), which in turn induces natural convection by the fluid within the cavity. The flow domain is a squared cavity with dimension L as shown in the left diagram of Fig. 1. The left and right vertical walls are maintained at dimensionless hot temperature $T_H = 0.5$ and cold temperature $T_C = 0.5$, respectively. The bottom and top horizontal walls are insulated, whereas no-slip boundary conditions are imposed for the fluid flow on all cavity walls. The Prandtl number Pr and the Rayleigh number Ra are defined as

$$Pr = \frac{v}{k}, \quad Ra = \frac{g\beta L^3 (T_H - T_C)}{v}.$$

This test problem has been extensively studied in the literature for non-radiating flows, see for example [12]. Here we also consider radiation effect in a non-scattering participating fluid. The left and right cavity walls are assumed to be diffusive to radiation such that boundary conditions for the radiative intensity are $I = B(T_H)$ and $I = B(T_C)$ on the left and right wall, respectively. Total reflection is imposed at the top and

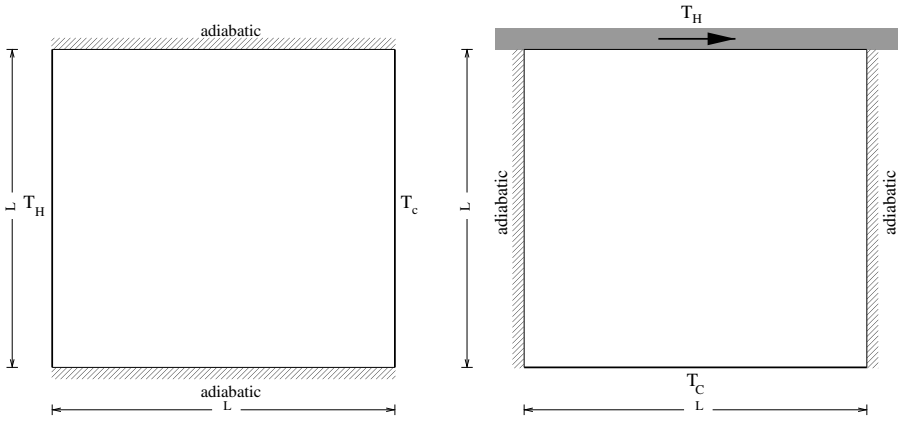

Fig. 1. Geometry of test problem for the natural (left) and forced (right) convection–radiation.

bottom cavity walls. We present computational results for the Prandtl number $Pr = 0.71$ and absorption coefficient $\sigma_a = 1$ with Rayleigh numbers Ra ranging from 10^4 to 10^7. In order to evaluate the heat transfer rate along the hot wall, we calculate the local Nusselt number, Nu_H, and its averaged value, $\overline{Nu}_H$, as

$$Nu_H(y) = \frac{L}{T_H - T_C}\left.\frac{\partial T}{\partial x}\right|_{x=0}, \quad \overline{Nu}_H = \frac{1}{L}\int_0^L Nu_H(y)\,dy.$$

A series of computations was done for the selected set of parameters to determine effects of the grid on the solution. We have considered four meshes with 32×32, 64×64, 128×128 and 256×256 gridpoints. In Fig. 2 we show the local Nusselt numbers at the hot wall and cross sections of the temperature at mid-height cavity

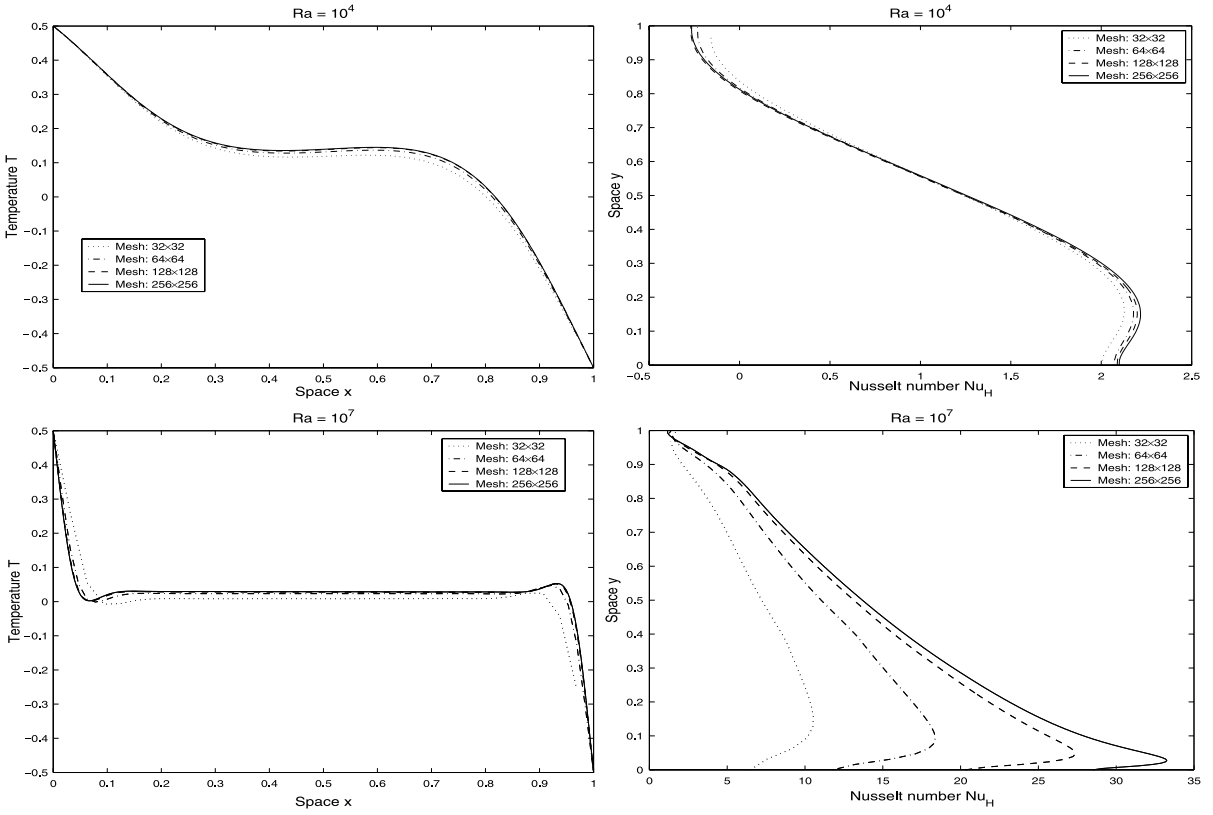

Fig. 2. Local Nusselt numbers at the hot wall (right column) and cross sections of the temperature at mid-height cavity (left column) for $Ra = 10^4$ and $Ra = 10^7$.

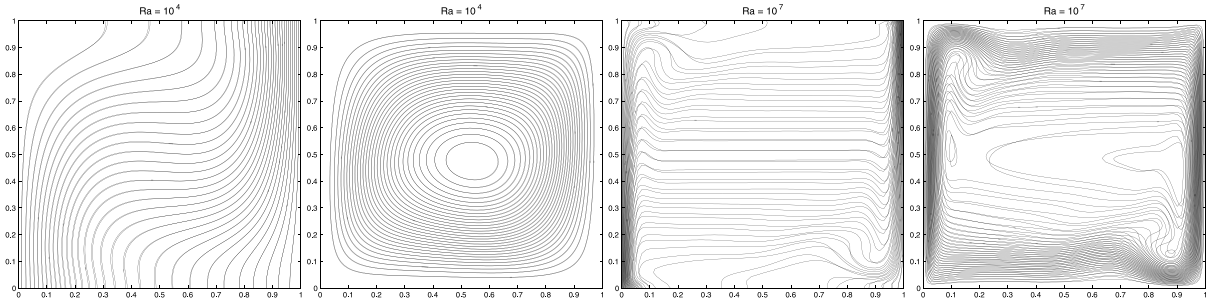

Fig. 3. Accuracy comparisons between second-order reconstruction (dashed lines) and third-order reconstruction (solid lines) for $Ra = 10^4$ and $Ra = 10^7$.

t that th ture is in
the ove pattern and
n the ca n both calcu-
ortex is ated at the mid-
the vo tex center moves to
h te perature distribution
er radiation at different

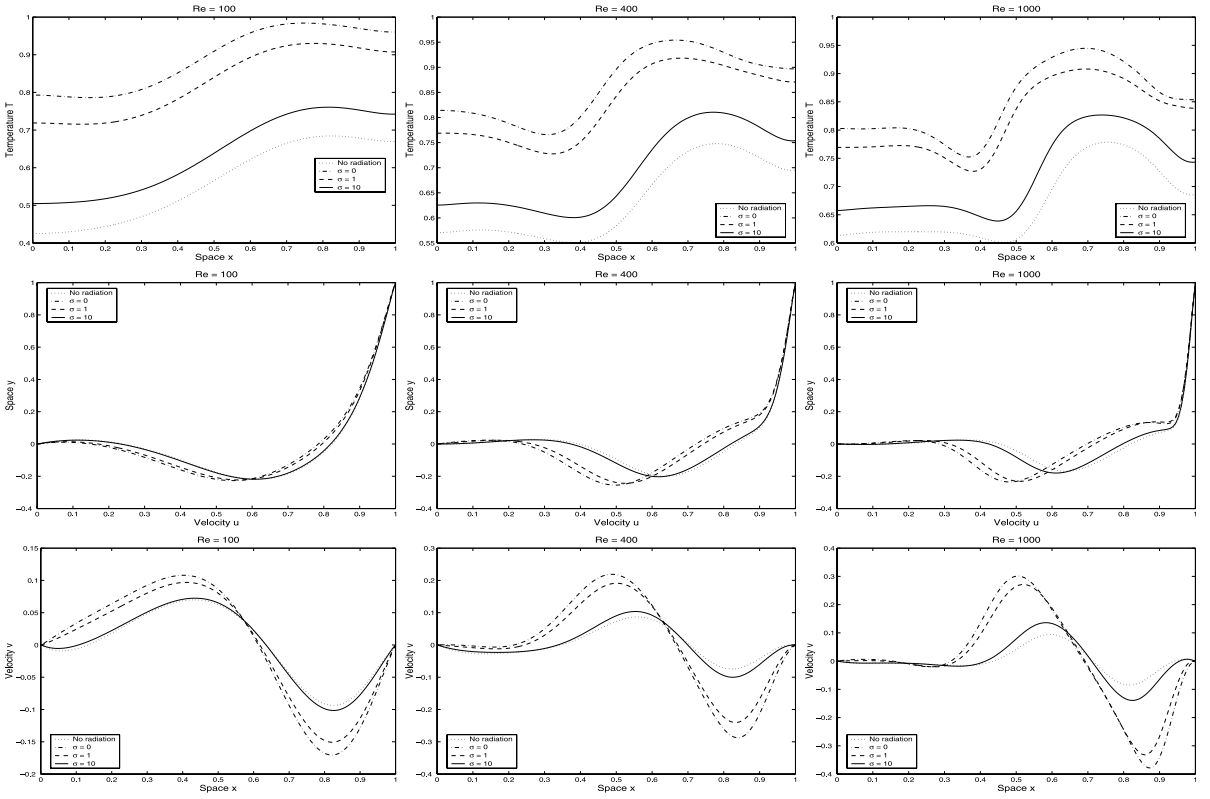

Fig. 11. Comparison results for forced convection without and with radiation using different scattering coefficients and Reynolds numbers.

crete-velocity models and relaxation schemes accurately approximate the numerical solution of this forced convection–radiation problem.

As a final remark, we want to comment on the computational work referred to CPU times for the presented models. In our implementation, the additional CPU time required to carry out a step in the coupled convection–radiation model with $\sigma_a = 0$, $\sigma_a = 1$ and$\sigma_a = 10$ is about 13%, 21% and 63% more costly than a computational step in no-radiation simulation. It is also important to mention two points concerning the DSA method for solving radiative transfer. First, the DSA method requires a large number of iterations only in the scattering-dominated computations. Otherwise, five iterations were sufficient to reach the tolerance of 10^{-6} for low-scattering computations. Second, for total reflective boundary conditions, an extra iterative process has to be added to the DSA iteration, which may result in an increase of computational cost.

5. Concluding remarks

In this work, a class of lattice-Boltzmann discrete-velocity moment models for coupled convection and radiation systems have been derived and a third-order relaxation method for solving the systems has been developed. The mass, momentum and energy equations are obtained from the nine-velocity distributions of flow and temperature variables. Simplified relaxation systems have been formulated using a suitable scaling in the discrete-velocity equations. The radiation coupling is accounted for in the energy equation by considering the S_N-discrete radiative transfer in participating media. Natural and forced convection–radiation problems have been recovered in the relaxation limit. It has been shown that the lattice-Boltzmann discrete-velocity models reproduce all the known features of coupled convection–radiation phenomena in the relaxation limit.

To solve the relaxation systems numerically, we have implemented a third-order spatial reconstruction and a third-order IMEX time marching scheme. The main advantages of the proposed relaxation method are the

high resolution, due to the little amount of numerical dissipation, and its simplicity. No Riemann solvers or characteristic decompositions are involved in its reconstruction. The IMEX scheme allows for an implicit treatment of the stiff source terms without relying on nonlinear solvers or iterative procedures. At the zero relaxation limit the method reduces to a TVD explicit time stepping scheme for the incompressible Navier–Stokes equations. The performance of the resulting numerical models has been assessed in two test cases, natural convection–radiation and forced convection–radiation flows in a squared cavity. The results of these tests have shown the high accuracy of the employed schemes and their capabilities to solve thermal flows for all Rayleigh and Reynolds numbers considered. In addition, it has been observed that in both test cases, the temperature distribution and the velocity field are affected by the presence of radiation in the enclosures. Further investigation of the models using three-dimensional thermal flows with turbulence is underway and results will be presented in future.

Acknowledgments

The work by A. Klar and M. Seaïd is supported in part by the Deutsche ForschungsGemeinschaft in the collaborative research center SFB568 ''Flow and Combustion in Future Gas Turbine Combustion Chambers''. M.K. Banda is deeply grateful to the University of KwaZulu-Natal Competitive Grant 2006 ''Flow Models with Source Terms, Scientific Computing, Optimization in Applications'' for partial funding.

References

[1] D. Aregba-Driollet, R. Natalini, S.Q. Tang, Diffusive kinetic explicit schemes for nonlinear degenerate parabolic systems, Math. Comput. 73 (2004) 63–94.
[2] M.K. Banda, M. Seaïd, Higher-order relaxation schemes for hyperbolic systems of conservation laws, J. Numer. Math. 13 (2005) 171–196.
[3] M.K. Banda, M. Seaïd, A. Klar, L. Pareschi, Lattice-Boltzmann type relaxation systems and higher order relaxation schemes for the incompressible Navier–Stokes equation, Math. Comput. (in press).
[4] M.K. Banda, M. Seaïd, I. Teleaga, Discrete-velocity relaxation methods for large-eddy simulation, Appl. Math. Comput. 182 (2006) 739–753.
[5] C. Bardos, F. Golse, D. Levermore, Fluid dynamic limits of kinetic equations: formal derivations, J. Stat. Phys. 63 (1991) 323–344.
[6] R. Benzi, S. Succi, M. Vergassola, The lattice-Boltzmann equation: theory and applications, Phys. Rep. 222 (1992) 145–197.
[7] R.E. Caflisch, S. Jin, G. Russo, Uniformly accurate schemes for hyperbolic systems with relaxation, SIAM J. Numer. Anal. 34 (1997) 246–281.
[8] N. Cao, S. Chen, S. Jin, D. Martinez, Physical symmetry and lattice symmetry in lattice Boltzmann methods, Phys. Rev. E 55 (1997) R21–R24.
[9] H. Chen, S. Chen, W. Matthaeus, Recovery of the Navier–Stokes equations using a lattice-gas Boltzmann method, Phys. Rev. A 45 (1992) 5339–5342.
[10] S. Chen, G.D. Doolen, Lattice Boltzmann method for fluid flows, Ann. Rev. Fluid Mech. 30 (1998) 329–364.
[11] A. De Masi, R. Esposito, J.L. Lebowitz, Incompressible Navier–Stokes and Euler limits of the Boltzmann equation, Commun. Pure Appl. Math. 42 (1989) 1189–1214.
[12] D. De Valhl Davis, Natural convection of air in a square cavity: a benchmark solution, Int. J. Numer. Meth. Fluids 3 (1983) 249–264.
[13] F.J. Higuera, S. Succi, R. Benzi, Lattice gas dynamics with enhanced collision, Europhys. Lett. 9 (1989) 345–349.
[14] D. d'Humières, Generalized lattice-Boltzmann equations in AIAA rarefied gas dynamics: theory and applications, Prog. Astronaut. Aeoronaut. 159 (1992) 450–458.
[15] W. Fiveland, Discrete-ordinates solutions of the radiative transport equation for rectangular enclosures, J. Heat Transfer 106 (1984) 699–706.
[16] U. Ghia, K.N. Ghia, C.T. Shin, High-*Re* solutions for incompressible flow using the Navier–Stokes equations and multigrid method, J. Comput. Phys. 48 (1982) 387–411.
[17] L. Giraud, D. d'Humieres, P. Lallemand, A lattice Boltzmann model for Jeffreys viscoelastic fluid, Europhys. Lett. 42 (1998) 625–630.
[18] Z. Guo, B. Shi, C. Zheng, A coupled lattice BGK model for the Boussinesq equations, Int. J. Numer. Meth. Fluids 39 (2002) 325–342.
[19] X. He, S. Chen, G.D. Doolen, A novel thermal model for the lattice Boltzmann Method in incompressible Limit, J. Comput. Phys. 146 (1998) 282–300.
[20] X. He, L.S. Luo, A priori derivation of the lattice Boltzmann equation, Phys. Rev. E 55 (1997) 6333–6336.
[21] X. He, L.S. Luo, Lattice Boltzmann model for the incompressible Navier–Stokes equation, J. Stat. Phys. 88 (1997) 927–944.
[22] T. Inamuro, M. Yoshino, F. Ogino, Accuracy of the lattice Boltzmann method for small Knudsen number with finite Reynolds number, Phys. Fluids 9 (1997) 3535–3542.
[23] R. Iwatsu, J.M. Hyun, K. Kuwahara, Mixed convection in a driven cavity with a stable vertical temperature gradient, Int. J. Heat Mass Tranfer. 36 (1993) 1601–1608.

[24] S. Jin, Z. Xin, The relaxation schemes for systems of conservation laws in arbitrary space dimensions, Commun. Pure Appl. Math. 48 (1995) 235–276.
[25] M. Junk, A. Klar, L.-S. Luo, Asymptotic analysis of the lattice Boltzmann equation, J. Comput. Phys. 210 (2005) 676–704.
[26] A. Klar, An asymptotic-induced scheme for nonstationary transport equations in the diffusive limit, SIAM J. Numer. Anal. 35 (1998) 1073–1094.
[27] A. Klar, Relaxation schemes for a lattice Boltzmann type discrete velocity model and numerical Navier–Stokes limit, J. Comput. Phys. 148 (1999) 1–17.
[28] P.K. Kundu, I.M. Cohen, Fluid Mechanics, third ed., Elsevier, Oxford, 2004.
[29] L.D. Landau, E.M. Lifschitz, Fluid Mechanics Course of Theoretical Physics, second ed., vol. 6, Butterworths/Heinemann, London, 1987.
[30] F. Liotta, V. Romano, G. Russo, Central schemes for balance laws of relaxation type, SIAM J. Numer. Anal. 38 (2000) 1337–1356.
[31] F. Massaioli, R. Benzi, S. Succi, Exponential tails in two-dimensional Rayleigh–Bernard convection, Europhys. Lett. 21 (1993) 305–310.
[32] D. Mihalas, B.S. Mihalas, Foundations of Radiation Hydrodynamics, Oxford University Press, New York, 1983.
[33] M.F. Modest, Radiative Heat Transfer, McGraw-Hill, New York, 1993.
[34] L. Pareschi, G. Russo, Implicit–explicit Runge–Kutta schemes and applications to hyperbolic systems with relaxation, J. Sci. Comput. 25 (2005) 129–155.
[35] G. Puppo, F. Bianco, G. Russo, High order central schemes for hyperbolic system of conservation laws, SIAM J. Sci. Comput. 21 (1999) 294–322.
[36] Y.H. Qian, D. d'Humieres, P. Lallemand, Lattice BGK models for the Navier–Stokes equation, Europhys. Lett. 17 (1992) 479–484.
[37] M. Seaïd, M. Frank, A. Klar, R. Pinnau, G. Thömmes, Efficient numerical methods for radiation in gas turbines, J. Comput. Appl. Math. 170 (2004) 217–239.
[38] M. Seaïd, A. Klar, Asymptotic-preserving schemes for unsteady flow simulations, Comput. Fluids 35 (2006) 872–878.
[39] M. Seaïd, A. Klar, Efficient preconditioning of linear systems arising from the discretization of radiative transfer equation, Lect. Notes Comput. Sci. Eng. 35 (2003) 211–236.
[40] X. Shan, X. He, Discretization of the velocity space in the solution of the Boltzmann equation, Phys. Rev. Lett. 80 (1998) 65–68.
[41] Y. Shi, T.S. Zhao, Z.L. Guo, Thermal lattice Bhatnagar–Gross–Krook model for flows with viscous heat dissipation in the incompressible limit, Phys. Rev. E 70 (2004) 066310.
[42] Y. Shi, T.S. Zhao, Z.L. Guo, Finite difference-based lattice Boltzmann simulation of natural convection heat transfer in a horizontal concentric annulus, Comput. Fluids 35 (2006) 1–15.
[43] Y. Sone, Asymptotic theory of a steady flow of a rarefied gas past bodies for small Knudsen numbers, in: R. Gatignol, Soubbaramayer (Eds.), Advances in Kinetic Theory and Continuum Mechanics, Proceedings of a Symposium Held in Honour of Henri Cabannes (Paris), Springer, New York, 1990, pp. 19–31.